VNIVERSITAT DE VALÈNCIA

UNIVERSITAT POLITÈCNICA DE VALÈNCIA

Master Thesis - Year 2020/2021

Mathematical toolbox for singularity trajectories of an optical vectorial field

Author: **Sergio de María García**

Tutors:
Miguel Ángel García March
Carles Millán Enrique

Master's Degree in Mathematical Research

Abstract

The study of polarization singularities in complex fields has been booming in recent years. In this Master Thesis, we study a non-separable paraxial vector field and the phase and polarization singularities that it can show. We discuss the relationship between a multisingular initial field in each component (channel) and the polarization singularities. We describe two kinds of polarization singularities: those of circular polarization (C points) and those of linear polarization (L lines). We also classify the C points with a topological charge ± 1 in several ways (according to their charge, their contour and the number of major axes that will end up in it), and we define different phases for the case of singularities with a higher topological charge. We use the theory of the scattering modes to perform the dynamical evolution of the initial multisingular fields. We introduce a tool developed with the "Mathematica" software that allows one to perform this evolution and to visualise the phase and polarization singularities along evolution. We discuss the dynamics of many initial conditions, which allow us to illustrate the relationship between both kinds of singularities, and also the merging or disintegration of phase singularities along evolution.

Key words: Multisingular Gaussian beams; singular optics; polarization singularities

Index

Introduction

The method of analogies is a fruitful technique used in physics [1], and also in mathematics [2]. In the history of physics, a prominent example is the analogy between acoustics and optics, which ultimately led to many advancements in classical physics [3, 4]. Also, the birth and development of quantum physics are intimately related to its analogy to optics [5–9] . The study of phase singularities in optics [10–12] also was born from an analogy between these singularities in complex fields and dislocations in crystals [13–15]. A phase singularity occurs in those positions where the intensity of the complex field is zero and the phase is undetermined. Following circuits around these *dark spots* which are infinitely close to it, the phase increase in integer multiples of 2π. But singularities do not only appear in light beams. They also appear in other areas such as plasma physics [16], fluid physics [17] or atmospheric studies [18]. However, it became increasingly popular in the field photonics because complex waves can be encountered naturally. This led to the establishment of an independent branch of physics called *singular optics* [19–21].

One of the most important milestones in this field was when, in 1992, Allen et al. [22] showed that these phase singularities could also show an *orbital angular momentum* (OAM) [23–25]. This was extended to the case in which the system presents a discrete rotational symmetry [26], where the concept of orbital angular pseudo-momentum was introduced, even in the non-linear case [27–29]. Furthermore, it was also observed that the zeros of the solutions of the Helmholtz (2) equation create knots where the wave function vanishes (*knotted nothings*) as it evolved in time. Then, the study of this phenomena is very important in optical fields [30–33]. The field evolved including more and more concepts from topology, and the term *topological photonics* refers nowadays to a vast field which relates vortex and other topological properties [34, 35]. Interestingly, it has even been possible to go beyond the spatial and temporal dimensions to include synthetic dimensions [36].

Optical fields and their similarities between superfluids, superconductors and Bose-Einstein condensates have been studied [37–40]. Nowadays they are used for the study of solar rays [41–43] and even in medicine [44]. Many results which involve non-linear and discrete symmetry have been developed only for the scalar complex field case. The purpose of this work is to study singularities of complex vectorial fields. In such a case, there exist two kinds of singularities: (i) the aforementioned phase singularities and (ii) polarization singularities [45–47]. Here, we will study both kinds of singularities and set the framework to study (i) their dynamical evolution; (ii) phenomena associated to the presence of external

fields giving rise to discrete symmetry (similarly to the scalar case); and (iii) the extension to the non-linear case.

As we discused above, from a mathematical point of view these fields allow us to make a broad study using: (i) Differential equations, due to the equations we will use to parametrize, (ii) group theory, since we will use the groups SU(2) and SO(3) to be able to visualise and understand the fields better and (iii) topology, more specifically the fundamental group. We will use what is known in physics as the topological charge of a singularity.

In the scalar case we solve the paraxial diffraction equation

$$-ik_0 n\frac{\partial}{\partial z}\phi + \frac{1}{2}\nabla_t^2\phi = 0, \tag{1}$$

where k_0 is the ratio of the time frequency of a wave (ω) to the speed of light (c); and n is the ratio of the speed of light to the speed of propagation in the medium (v). The function ϕ can be written with the usual coordinates $\phi(x, y, z)$ or with the complex $\phi(w, \bar{w}, z)$ with $w = x+iy$ and $\bar{w} = x - iy$ its complex conjugate. The equation (1) is a paraxial approximation of the Helmholtz equation

$$\frac{\partial^2}{\partial z^2}U + \nabla_t^2 U + k_0^2 n^2 U = 0, \tag{2}$$

where $U(x, y, z) = \phi(x, y, z)e^{ik_0 nz}$.

In the case of a plane wave ($E = Ue^{-i\omega t}$) we have that if $U(x, y, z) = U_0 e^{i\vec{k}\cdot\vec{x}} = U_0 e^{ik_x x}e^{ik_y y}e^{ik_z z}$ and we substitute it in eq. (2), we obtain

$$\omega^2 = \frac{c^2}{n^2}(k_x^2 + k_y^2 + k_z^2). \tag{3}$$

Equation (2) is a specific case of the wave equation

$$\nabla^2 E - \frac{n^2}{c^2}\frac{\partial^2}{\partial^2}E = 0, \tag{4}$$

with $E(x, y, z, t) = U(x, y, z)e^{-i\omega t}$.

If $k_x + k_y + k_z$ is constant, then we obtain a plane and its stratifications where, for every λ, we would have a maximum of the function, because we are considering a plane wave (see Fig. 2). If we consider $\vec{k} = (0, 0, k_z)$, we have that $U(x, y, z) = U_0 e^{i\vec{k}\vec{x}} = U_0 e^{ik_z z}$, so the function $\phi(x, y, z) = U_0$, and if we consider the real part of U we will obtain a cosine (see Fig. 2)

In Fig. 3 we show a more realistic situation. In this case $\phi(x, y, z)$ is not constant and only depends on z [$\phi(z)$]. In this case $\lambda(z)$ is also a function of z. We will say that $\phi(z)$ depends smoothly on z or is a paraxial approximation if

$$\left|\frac{\partial^2\phi}{\partial z^2}\right| << k_0 n\left|\frac{\partial\phi}{\partial z}\right|, \tag{5}$$

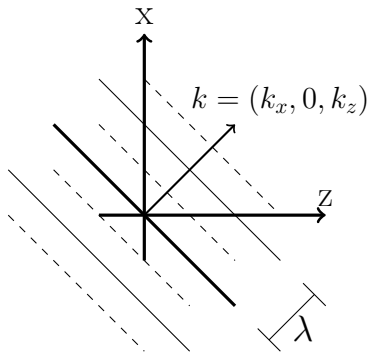

Figure 1: Plane wave with $k_y = 0$ with maxima with a continuous line and minima with a dashed line.

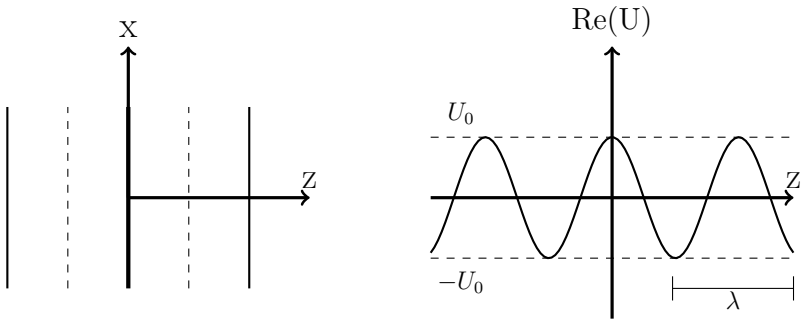

Figure 2: Plane wave with $k_x = k_y = 0$ propagating along the z-axis, and real part of the same field with maximums (minimums) in U_0 ($-U_0$).

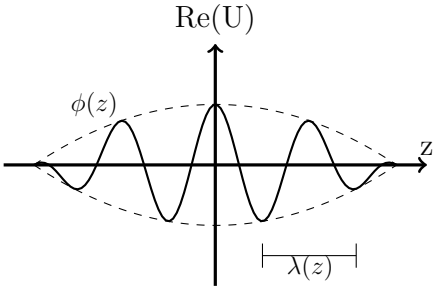

Figure 3: Real part of plane wave with $k_x = k_y = 0$ and being ϕ a function of z.

i.e. it is a negligible term. In this way we can transform the equation (2) into the equation (1) because the term $\frac{\partial^2 \phi}{\partial z^2}$ is cancelled.

It is easy to see that a solution of Equation (1) is proportional to e^{iF}, where F is a real function known as phase. Then the topological charge is defined as

$$N = \frac{1}{2\pi} \oint_C \nabla F(r) dr, \tag{6}$$

where C is a sufficiently small closed curve around the singularity, and $N \in \mathbb{Z}$, in other words, it is quantized.

In this work we are going to study the non-separable paraxial vector fields, and for this, in chapter 1 we will see which equations we will use to model our field, place singularities and evolve the vectorial field along the z direction. In this part we will follow the theory introduced in [48]. In the second chapter we will see how to visualise our field in different ways. We will also define the object of study of this work, the singularities. In chapter 3 we will define the simplest type of singularities ways. We will also discuss how we can classify them. In chapter 4 we will study singularities with higher topological loadings and how we can extract information from them with the line integrals taken from [46]. And finally, in chapter 5 we will see the results that the tool that we have created with all the previous information gives us. We will offer some conclusions and outlook in chapter 6.

Chapter 1

Scattering modes

1.1 Scattering modes

Let us first define how to mathematically parametrize a complex scalar field and their singularities following the formalism described in [48]. This aproach enables us to evolve the fields along the z-direction and allows us to introduce the extension to the vectorial case. We will solve the paraxial diffraction equation

$$-2ik_0\frac{\partial\phi}{\partial z}+\nabla_t^2\phi=0, \tag{1.1}$$

where the function $\phi:\mathbb{C}\times\mathbb{R}\to\mathbb{C}$ is the complex field, $\nabla_t\equiv(\partial/\partial x,\partial/\partial y)$ is the transverse gradient operator and k_0 is the light wavenumber, and it verifies the initial condition at $z=0$

$$\Phi_{lp}(r,\theta,0)=r^{|l|+2p}\exp(il\theta)\exp\left[-\frac{k_0r^2}{2z_R}\right], \tag{1.2}$$

where z_R is the Rayleigh length. We can rewrite eq.(1.2) in the complex variables $w=x+iy$ and $\bar{w}=x-iy$ as

$$\begin{aligned}\Phi_{lp}(w,\bar{w},0)&=w^{|l|}|w|^{2p}\exp\left[-\frac{k_0r^2}{2z_R}\right] \quad l\geq 0,\\ \Phi_{lp}(w,\bar{w},0)&=\bar{w}^{|l|}|w|^{2p}\exp\left[-\frac{k_0r^2}{2z_R}\right] \quad l<0.\end{aligned} \tag{1.3}$$

We now define the complex position operator $\hat{w}$ and $\hat{\bar{w}}$ and their respective momentum operators $\hat{p}=-i\partial/\partial w$ and $\hat{\bar{p}}=-i\partial/\partial\bar{w}$, which commutations relation [1] are

$$\begin{aligned}[\hat{w},\hat{p}]&=\hat{w}\hat{p}-\hat{p}\hat{w}=-i\overbrace{\hat{w}\frac{\partial}{\partial w}}^{0}+i\frac{\partial}{\partial w}\hat{w}=i,\\ [\hat{\bar{w}},\hat{\bar{p}}]&=\hat{\bar{w}}\hat{\bar{p}}-\hat{\bar{p}}\hat{\bar{w}}=-i\overbrace{\bar{w}\frac{\partial}{\partial\bar{w}}}^{0}+i\frac{\partial}{\partial\bar{w}}\hat{\bar{w}}=i.\end{aligned} \tag{1.4}$$

[1] The commutator function between two operators $\hat{A},\hat{B}$ is defined as $[\hat{A},\hat{B}]=\hat{A}\hat{B}-\hat{B}\hat{A}$

Thus, we can write the Hamiltonian associated with (1.1) as $\hat{H} = \hat{p}\hat{\bar{p}}$, and the operator that allows us to evolve along the z-direction $\hat{U}(z) = \exp[i(2z/k_0)\hat{H}]$, satisfying

$$\begin{aligned} [\hat{w}, \hat{U}(z)] &\overset{2}{=} -(2z/k_0)\hat{\bar{p}}\hat{U}(z), \\ [\hat{w}, \hat{U}(z)] &= -(2z/k_0)\hat{p}\hat{U}(z). \end{aligned} \tag{1.5}$$

Thus, using these commutation relations it is possible to obtain a solution of the equation (1.1) for a initial initial vortex state at any given z. Such solution can be written as

$$\Phi_{lp}(r,\theta,z) = w^{|l|}\left(\frac{iz_R}{q(z)}\right)^{|l|+1}\left(\frac{2zz_R}{k_0 q(z)}\right)F_p^{|l|}(\gamma(z)|w|^2)r^{|l|}\exp(il\theta)\exp\left[-i\frac{k_0|w|^2}{2q(z)}\right], \tag{1.6}$$

for $l \geq 0$, and

$$\Phi_{lp}(r,\theta,z) = \bar{w}^{|l|}\left(\frac{iz_R}{q(z)}\right)^{|l|+1}\left(\frac{2zz_R}{k_0 q(z)}\right)F_p^{|l|}(\gamma(z)|w|^2)r^{|l|}\exp(il\theta)\exp\left[-i\frac{k_0|w|^2}{2q(z)}\right], \tag{1.7}$$

for $l < 0$, where $q(z) = z + iz_R$, $\gamma(z) = (k_0/2)z_R[zq(z)]^{-1}$ and $F_p^{|l|}$ are polynomials of pth order knows as *F-polynomials*. These polynomials satisfy the recurrence relations

$$F_{p+1}(x) = (1-x)F_p(x) - (1-2x)\frac{dF_p(x)}{dx} - x\frac{d^2F_p(x)}{dx^2}, \tag{1.8}$$

for $p = 0, 1, 2, \ldots$ where $F_0(x) = 1$, and

$$F_p^{|l|+1}(x) = F_p^{|l|}(x) - \frac{dF_p^{|l|}(x)}{dx}, \tag{1.9}$$

for $|l| = 0, 1, 2, \ldots$ where $F_p^0(x) = F_p(x)$.

The solution can be found in [48], and in table 1.1 are tabulated the polynomials for the degrees we are going to use in this work.

1.2 Vector case

Let us extend the provious theory to the vector case. The wave equation in the vector case is similar to (4). It reads as

$$\nabla^2\vec{E} + \frac{n^2}{c^2}\frac{\partial^2}{\partial t^2} = 0, \tag{1.10}$$

[2] If $[A, B] = k$, then $[A, \exp(\lambda B)] = \lambda k \exp(\lambda B)$

$F_p^1(x)$
$F_0^1(x) = 1$
$F_1^1(x) = 2 - x$
$F_2^1(x) = 6 - 6x + x^2$
$F_3^1(x) = 24 - 36x + 12x^2 - x^3$
$F_4^1(x) = 120 - 240x + 120x^2 - 20x^3 + x^4$
$F_p^2(x)$
$F_0^2(x) = 1$
$F_1^2(x) = 3 - x$
$F_2^2(x) = 12 - 8x + x^2$
$F_3^2(x) = 60 - 60x + 15x^2 - x^3$
$F_4^2(x) = 360 - 480x + 180x^2 - 24x^3 + x^4$
$F_p^3(x)$
$F_0^3(x) = 1$
$F_1^3(x) = 4 - x$
$F_2^3(x) = 20 - 10x + x^2$
$F_3^3(x) = 120 - 90x + 18x^2 - x^3$
$F_4^3(x) = 840 - 840x + 252x^2 - 28x^3 + x^4$
$F_p^4(x)$
$F_0^4(x) = 1$
$F_1^4(x) = 5 - x$
$F_2^4(x) = 30 - 12x + x^2$
$F_3^4(x) = 210 - 126x + 21x^2 - x^3$
$F_4^4(x) = 1680 - 1344x + 336x^2 - 32x^3 + x^4$

Table 1.1: Generalized F-polynomials for $l = 1, 2, 3, 4$ and $p = 0, 1, 2, 3, 4$

where $\vec{E} : \mathbb{R}^3 \to \mathbb{C}$ is a electric field. In this case we have one more condition given by Maxwell's equations. This equation binds the components through $\vec{\nabla} \cdot \vec{E} = 0$ because there are no sources of the magnetic field and the medium is homogeneous. This bound can be translated into $\vec{k} \cdot \vec{E} = 0$.

If we consider $\vec{k} = (0, 0, k_z)$ as before, by this bound we have that $E_z(t) = 0$, i.e., the field propagates temporarily only in E_x and E_y. Therefore, at $z = 0$

$$\vec{E}(x, y, 0, t) = \vec{U}_0 \overbrace{e^{ik_z z}}^{1} e^{-i\omega t} = \begin{pmatrix} U_{0x} \\ U_{0y} \\ 0 \end{pmatrix} e^{-i\omega t}. \tag{1.11}$$

Similar to the scalar case, we consider the plane wave ($k_z = k_0 n$, with k_0 constant) $\vec{U}(x, y, z) = \vec{\Phi}(x, y, z)e^{ik_0 nz}$ which will now have 3 components. Then this function satisfies the Helmholtz vector equation

$$\frac{\partial^2}{\partial z^2}\vec{U} + \nabla_t^2\vec{U} + k_0^2 n^2 \vec{U} = 0, \tag{1.12}$$

and considering that it is a paraxial approximation, we get the equations

$$\left\{ \begin{array}{rcl} -ik_0 n\frac{\partial}{\partial z}\Phi_x + \frac{1}{2}\nabla_t^2\Phi_x &=& 0, \\ -ik_0 n\frac{\partial}{\partial z}\Phi_y + \frac{1}{2}\nabla_t^2\Phi_y &=& 0, \\ -ik_0 n\frac{\partial}{\partial z}\Phi_z + \frac{1}{2}\nabla_t^2\Phi_z &=& 0. \end{array} \right. \tag{1.13}$$

Now, contour equation becomes $0 = \nabla \cdot \vec{E} = \partial_z\phi_z + \partial_+\phi_- + \partial_-\phi_+$ (where $\phi_\pm = \phi_x \pm \phi_y$), and taking into account the paraxial approximation

$$ik_0 n\phi_z = -(\partial_+\phi_- + \partial_-\phi_+) = -(\partial_x\phi_x + \partial_y\phi_y). \tag{1.14}$$

Therefore, it is enough to propagate it in ϕ_x and ϕ_y, and ϕ_z would be calculated using them and equation (1.14), which is a consequence of the bound $\vec{k}\cdot\vec{E} = 0$, so we will call it bound condition.

Let us consider the moment operators in Cartesian coordinates ($\hat{p}_x$ and $\hat{p}_y$), it is easy to see that $\hat{p}\hat{\bar{p}} = \hat{p}_x^2 + \hat{p}_y^2$, so we can write the operator $\hat{U}(z)$ as

$$\hat{U}(z) = e^{i\frac{\hat{p}\hat{\bar{p}}}{2}z} = e^{i\frac{\hat{p}_x^2+\hat{p}_y^2}{2}z}. \tag{1.15}$$

The operators $\hat{p}_x^2$ and $\hat{p}_y^2$ commute with each other, so they also commute with the operator $\hat{U}(z)$

$$[\hat{U}(z), \hat{p}_x^2] = [e^{i\frac{\hat{p}_x^2+\hat{p}_y^2}{2}z}, \hat{p}_x^2] = \frac{iz}{2}[\hat{p}_x^2 + \hat{p}_y^2, \hat{p}_x^2]\hat{U}(z) = 0, \tag{1.16}$$

and analogously with the operator for y.

Thus, if we have that the initial equation is satisfied for $z = 0$, then we can apply the operator $\hat{U}(z)$ and it will be satisfied for all $z \geq 0$.

$$\begin{aligned} ik_0 n\phi_z(0) &= -(\partial_x\phi_x(0) + \partial_y\phi_y(0)), \\ ik_0 nU(z)\phi_z(0) &= -U(z)(i\hat{p}_x\phi_x(0) + i\hat{p}_y\phi_y(0)), \\ ik_0 n\phi_z(z) &= -i(U(z)\hat{p}_x\phi_x(0) + U(z)\hat{p}_y\phi_y(0)), \\ ik_0 n\phi_z(z) &= -i(\hat{p}_x U(z)\phi_x(0) + \hat{p}_y U(z)\phi_y(0)), \\ ik_0 n\phi_z(z) &= -i(\hat{p}_x\phi_x(z) + \hat{p}_y\phi_y(z)). \end{aligned} \tag{1.17}$$

Hence the equations (1.13) and (1.14) are satisfied, so we can make a similar development to the scalar case to solve it

$$\left.\begin{array}{rcl} \phi_+(0) &=& P_+(\omega,\bar{\omega})\phi_{00}, \\ \phi_-(0) &=& P_-(\omega,\bar{\omega})\phi_{00}, \end{array}\right\} \tag{1.18}$$

$$\phi_z(0) = \frac{i}{k_0 n}(\partial_+\phi_- + \partial_-\phi_+) = P_z(\omega, \bar{\omega})\phi_{00}(0). \tag{1.19}$$

Therefore, we can replicate the already known method.

Chapter 2

Polarization field

2.1 Polarization ellipses

In this section, we will introduce the peculiarities of the vectorial complex field, in constrast to a scalar complex field. Particularly, we will introduce the concept of polarization singularity. Let $\vec{E}$ be a complex vector wavefield. We can write it in cartesian or real and imaginary components $\vec{E}(x,y) = (E_x, E_y) = p(x,y) + iq(x,y)$, where $p, q \in \mathbb{R}^2$.

We are going to consider a monochromatic wave. Then, its time dependence is given by a phase factor $\exp(-i\omega t)$, where ω is the angular frequency associated with the field. The part of interest to us is the real part of the wavefield, i.e

$$\mathrm{Re}(\vec{E}) = \mathrm{Re}(|\vec{E}|e^{-i\theta}) = p\cos(\theta) + q\sin(\theta), \tag{2.1}$$

where $\theta = \omega t$. It is easy to see that $\mathrm{Re}(\vec{E})$ sweeps out an ellipse from its centre, as θ increases. The orthogonal semiaxes of the ellipse are p_0 and q_0 ($p_0 \geq q_0$) (see Fig. 2.1).

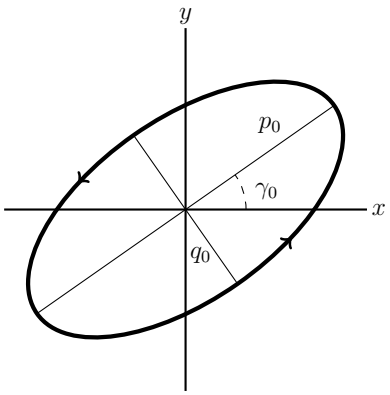

Figure 2.1: Right-handed ellipse with main axis p_0 is at angle γ_0 with the x-axis.

When the ellipse rotates anticlockwise as θ increases then $\vec{E}$ is said to be *right-handed* (RH); and, if it rotates clockwise, *left-handed* (LH). If $\vec{E}$ is RH, the cross product $\mathrm{Im}(\vec{E}^* \times \vec{E}) = 2(p \times q)$ is positive, and if E is LH, it is negative.

Let us define other coordinates with which we can more easily see if $\vec{E}$ is RH or LH. We are going to use the polar coordinates, defined by

$$e^+ = \frac{1}{\sqrt{2}} \begin{pmatrix} 1 \\ i \end{pmatrix} \quad e^- = \frac{1}{\sqrt{2}} \begin{pmatrix} 1 \\ -i \end{pmatrix}. \tag{2.2}$$

Now, $\vec{E}$ may be rewritten as $\vec{E} = E^+e^+ + E^-e^-$, where E^+, E^- are the right-handed and left-handed circular components of $\vec{E}$, and their phases are α^+, α^- respectively, and we can define the topological charge (6) for each of the components as

$$N^{\pm} = \frac{1}{2\pi} \oint_C \nabla \alpha^{\pm}(r) dr. \tag{2.3}$$

Therefore, there is a special phase χ_0 such that the real and imaginary parts of $|\vec{E}| \exp(-i\chi_0)$ are perpendicular. As can be seen in [45], we can write this phase as

$$\chi_0 = \frac{1}{2} \arctan \frac{2p \cdot q}{|p|^2 - |q|^2} = \frac{1}{2} \frac{\mathrm{Im}(E^+E^-)}{\mathrm{Re}(E^+E^-)} = \frac{1}{2} \arg(E^+E^-) = \frac{\alpha^+ + \alpha^-}{2}. \tag{2.4}$$

In [49], Nye called χ_0 the "phase of the vibration". The orientation of the ellipse defines the angle γ_0 given by the x-axis and the main axis p_0. And we can write it in terms of the field in the same way as in the previous case

$$\gamma_0 = \frac{1}{2} \arctan \frac{2(p_x p_y + q_x q_y)}{p_x^2 + q_x^2 - p_y^2 - q_y^2} = \frac{1}{2} \frac{\mathrm{Im}(E^{+*}E^-)}{\mathrm{Re}(E^{+*}E^-)} = \frac{1}{2} \arg(E^{+*} * E^-) = \frac{\alpha^- - \alpha^+}{2}. \tag{2.5}$$

The *polarization matrix (Stoke matrix or coherence matrix)* $\mathscr{M}_S$ is a 2×2 hermitian matrix defined by

$$(\mathscr{M}_S)_{ij} = E_i E_j^* \qquad i, j = x, y.$$

The real part of the *polarization matrix* ($\mathscr{M} = \mathrm{Re}(\mathscr{M}_S)$) is a positive definite symmetric matrix whose eigenvectors are in the directions of the axes of the ellipse p_0, q_0, and whose eigenvalues are $|p_0|^2$ and $|q_0|^2$, respectively. The four components of the $\mathscr{M}$ concerning the usual Pauli spin matrices [1] are known as the *Stokes parameters* S_0, S_1, S_2, S_3

$$\mathscr{M} = \begin{pmatrix} S_0 + S_1 & S_2 - iS_3 \\ S_2 + iS_3 & S_0 - S_1 \end{pmatrix}, \tag{2.6}$$

[1] Pauli matrices are 2 by 2 hermitian unitary complex matrices which form a basis of the Lie algebra of the special unitary group SU(2).

and they are given by

$$\begin{aligned} S_0 &= |E^+|^2 + |E^-|^2 = |E_x|^2 + |E_y|^2, \\ S_1 &= 2\mathrm{Re}(E^{+*}E^-) = |E_x|^2 - |E_y|^2, \\ S_2 &= 2\mathrm{Im}(E^{+*}E^-) = 2\mathrm{Re}(E_x^* E_y), \\ S_3 &= |E^+|^2 - |E^-|^2 = 2\mathrm{Im}(E_x^* E_y), \end{aligned} \tag{2.7}$$

where S_0 represents the intensity of the field $|E|$, $\pi|S_3|/2$ is the area of the polarization ellipse and the sign of S_3 gives the handedness of the ellipse, + for RH and - for LH.

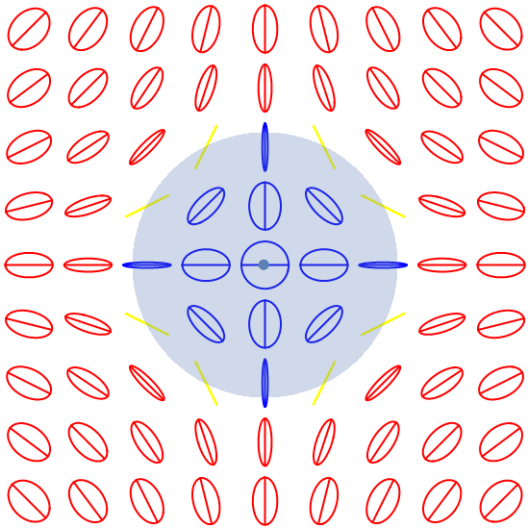

Figure 2.2: Optical field with a C point at the origin with topological charge -2. The red ellipses are RH elipses, the blue ones are LH elipses and the yellow ones have an excentricity less than 10^{-2}, i.e are near the L line which separates the southern hemisphere of the Poinacare sphere (blue background) from the northern hemisphere (white background).

Another motivation for defining the parameters in this way is that they satisfy

$$S_0^2 = S_1^2 + S_2^2 + S_3^2. \tag{2.8}$$

Then we can normalize the parameters $s_i = S_i/S_0$, $i = 1, 2, 3$ and now, we have a vector in the unit sphere S^2 called (normalized) *Stokes vector*. This is a different way to study and visualize the ellipse in each point on the field like a vector (or a point in the sphere).

Thus, the different states of polarization are parameterized by positions on the unit sphere, called *Poincaré sphere*. We can parametrize all possible polarization ellipses by the spherical polar angles δ and μ. The polar angle $\delta = \arccos s_3$ indicates the eccentricity of the ellipse, being 0 at the poles (circular polarization) and it increases gradually to 1 (linear

polarization) on the equator. When it is in the northern hemisphere ($S_3 > 0$), the handedness is RH and in the southern ($S_3 < 0$), it is LH. The azimuthal angle $\mu = 2\gamma_0 = \arctan s_2/s_1$ indicates the orientation of the main axis of the ellipse (see Fig.2.3).

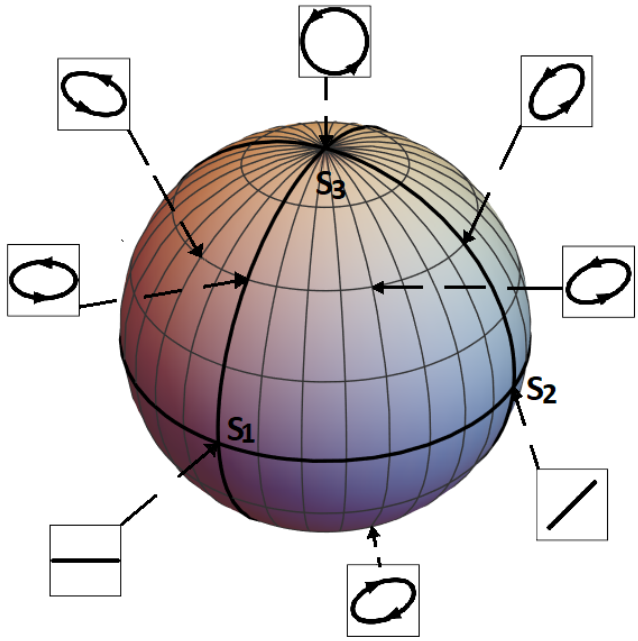

Figure 2.3: Poincaré sphere with ellipses in different positions

2.2 Polarization singularities

With all this knowledge, let us discuss about the points where the polarization ellipse "is no longer an ellipse": it becomes a circle (C points) or a straight line (L lines) (see Fig. 2.2).

2.2.1 C points

The points where the polarization is circular (either RH or LH) are known as C points, the most important type of polarization singularities. In a paraxial vector field, these C singularities have codimension 2, that is why it usually occurs in points.

There are different ways of considering these points:

- There will be a circumference when the real and imaginary vectors p, q are of equal length and orthogonal. It is equivalent to

$$\begin{array}{rcll} |p|^2 - |q|^2 & = & 0 & \text{(equal length)}, \\ 2(p \cdot q) & = & 0 & \text{(orthogonal)}. \end{array} \tag{2.9}$$

These equations are equivalent to the fact that the rectifying phase χ_0 (2.4) is undefined at the C point.

- Another way is to find the points where the Stokes parameters S_1, S_2 vanish. The points on the Poincaré sphere where the polarization is circular are the north and south poles where $S_1 = S_2 = 0$ and $S_3 = \pm S_0$ by (2.8). The C point is RH if $S_3 = S_0$, and LH if $S_3 = S_0$. The azimuthal μ (and orientation angle γ_0) is singular at the poles of the Poincaré sphere (there is no unicity in the axes of a ellipse). The singularity of γ_0 is different from that χ_0, although the two singularities always occur together.

- When the real symmetric matrix $\mathscr{M}$ is degenerate (combining the previous point and the definition (2.6)). The structure of these matrices around the singularity is called a *diabolical point* because the two eigenvalues locally have a double cone structure (diabolo). In [47], they use this to define the C-points of a real function f as degeneracies of its hessian matrix $\mathscr{H} = f_{ab}(a, b, = x, y)$

- Finally, we can consider the circular components E^+, E^-, the simplest and possibly most instructive way of viewing C points. We have a RH circular polarization where $E^- = 0$ and a LH circular polarization where $E^+ = 0$. Then, the phases α^-, α^+ are singular at the respective C points. This implies for (2.4) and (2.5), rectifying angle χ_0 and the ellipse orientation γ_0 are undefined at a C point.

2.2.2 L lines

Another type of singularity is the places where the ellipse turns into a line, that is, the places with linear polarization where the Stokes parameter $S_3 = 0$. The location where this happens has codimension 1, what is called L lines. L lines separate regions of RH and LH polarization and on these lines, the handedness of the ellipse is not defined. In terms of circular components, this implies that $|E^+| = |E^-|$ on an L line.

In contrast to the rich topological structure of the C points, there is no characteristic structure around an L line where generically S_3 passes through zero smoothly, and the phases change smoothly along the singular line. That is the reason why we are going to study only the C points in this paper.

Chapter 3

Classification of the simplest regular points

Now, we will discuss the topology structure around the simplest regular points and how we can classify the C points in terms of the ellipse surrounding them.

We have seen in the previous chapter that the phase γ_0 is singular in the C points, this implies that the line integral on a loop $\mathcal{L}$ around a C point

$$\Phi_C = \oint_{\mathcal{L}} \nabla\gamma_0 \, dR = \frac{1}{2} \oint_{\mathcal{L}} (\nabla\alpha^- - \nabla\alpha^+) \, dR = \pi N_C, \tag{3.1}$$

where $N_C \in \mathbb{Z}$ as in (6).

The number $N_C/2$ is known as the *topological index* of the C point. There is a simpler way to calculate the sign of the index knowing that it is the same as the sign of the function (3.1)

$$D_I = S_{1x}S_{2y} - S_{1y}S_{2x}. \tag{3.2}$$

In this chapter, we will work with the number N_C only, more precisely, the C points with topological index $\pm 1/2$.

So far, we can classify the simplest C points in four types, according to the handedness (RH or LH) and index ($\pm 1/2$)

3.1 Contour classification

We can classify the C point in elliptic or hyperbolic depending on whether the contour lines of the eigenvalues of $\mathscr{M}$ (2.6) around the singularity are ellipses or hyperbolas.

In [50], the function D_C determines the classification in terms of the Stokes parameters

$$D_C = (S_{1x}S_{2y} - S_{1y}S_{2x})^2 - (S_{1x}S_{0y} - S_{1y}S_{0x})^2 - (S_{0x}S_{2y} - S_{0y}S_{2x})^2. \tag{3.3}$$

When $D_C < 0$, the point is hyperbolic, and elliptic if $D_C > 0$.

To the best of our knowledge, it is not clear if there is a straightforward physical interpretation of this classification for C points.

3.2 Line classification

Let us remember that the C points are singularities of the orientation angle γ_0, which define the inclination of the main axis of the polarization ellipse with respect to the x-axis, i.e, it gives us an undirected line at each point.

The configuration of these lines is the key to classify the C points. Line fields can be classified depending on two things:

- If a line turns around the singularity anticlockwise (+) or not (-); that is, the sign of the index of the singularity, before returning to the same point.
- The number of straight lines that end on C points. In the simplest case that we study in this chapter, this number is 1 or 3, but we will see later that it may be changed.

Therefore, for index -1/2 the number of straight lines is always 3 and the singularity is called a *star*. And for index +1/2, it may be 1 or 3, and the singularity is called *lemon* or *monstar* respectively [45] (see Fig.3.1).

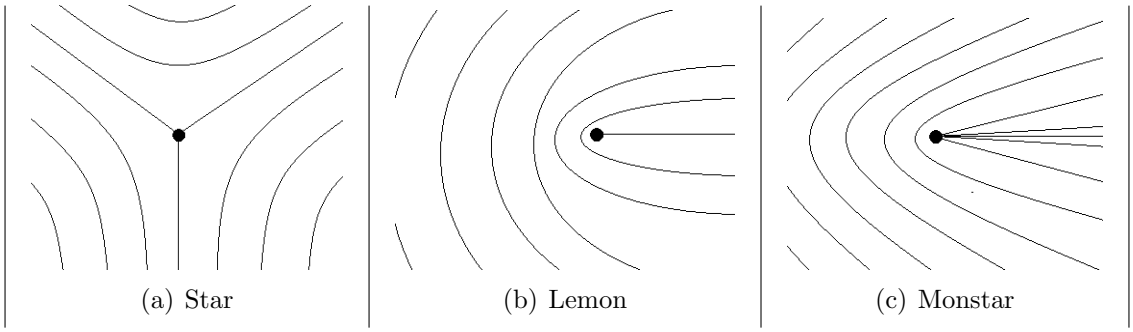

(a) Star (b) Lemon (c) Monstar

Figure 3.1: Types of C-points and the pattern that make the semi-major axes of ellipses around them.

There is a similar value to (3.2) whose sign gives the number of straight lines. We are going to define an equivalent expression to that of [50]. We want the places where the γ_0 is constant when we move away from the singularity. To simplify calculations, the C point translated to the origin, then we expand S_1, S_2 in $\gamma_0 = \arctan(S_2/S_1)/2$ to first order with polar coordinates R and angle $\theta = \arctan(y/x)$. We can rewrite this expression into a polynomial equation with $t = \tan\theta$

$$S_{2y}t^3 + (S_{2x} + 2S1y)t^2 + (2S_{1x} - S_{2y})t - S_{2x} = 0. \tag{3.4}$$

The solutions of (3.4) give the lines ending at the singularity. In order to determine the number of lines, we observe the discriminant of the polynomial is

$$\begin{aligned} D_L = ((2S_{1y} + S_{2x})^2 - 3S_{2y}(2S_{1x} - S_{2y})) \cdot ((2S_{1x} - S_{2y})^2 + 3S_{2x}(2S_{1y} + S_{2x})) \\ - (2S_{1x}S_{1y} + S_{1x}S_{2x} - S_{1y}S_{2y} + 4S_{2x}S_{2y})^2. \end{aligned} \tag{3.5}$$

If $D_L > 0$ there are 3 real roots, and if $D_L < 0$, only one. In the case that $D_L = 0$ we have no conclusive criteria.

Chapter 4

Phases of the field

We have seen how to classify the simplest singularities with index $\pm 1/2$. Now we will define some values that give us information about the singularity regardless of its index. Analogous to (3.1), we can define the dynamical phase N_D [46] because χ_0 is also singular at the C points

$$\Phi_D = \oint_{\mathcal{L}} \nabla\chi_0 \, dR = \frac{1}{2} \oint_{\mathcal{L}} (\nabla\alpha^+ + \nabla\alpha^-) \, dR = \pi N_D, \tag{4.1}$$

where $N_D \in \mathbb{Z}$ as (3.1) and (6), and it is known as the *topological number*. It is easy to check that the parity between N_D and N_C is the same because

$$\frac{N_D}{2} = \frac{N^+ + N^-}{2} \qquad \frac{N_C}{2} = \frac{N^- - N^+}{2}, \tag{4.2}$$

then

$$N_C \bmod 2 = N_D \bmod 2 \Longrightarrow \Phi_C \bmod 2\pi = \Phi_D \bmod 2\pi. \tag{4.3}$$

We can also obtain the total phase increment from the circular basis

$$\Phi = \oint \frac{E^*\dot{(\nabla)}E}{|E|^2} dR = \oint \frac{|E^+|^2\nabla\alpha^+ + |E^-|^2\nabla\alpha^-}{|E^+|^2 + |E^-|^2} dR. \tag{4.4}$$

Generally, this phase is not quantized, i.e, there is no integer N such that $\Phi = 2\pi N$. We can define another phase as the difference between the total phase (4.4) and the dynamical phase (4.1)

$$\Phi_G = \Phi - \Phi_D = \frac{1}{2} \oint \frac{|E^+|^2 - |E^-|^2}{|E^+|^2 + |E^-|^2} (\nabla\alpha^+ - \nabla\alpha^-) dR. \tag{4.5}$$

This phase is known as the *geometric phase*, and it is associated with the evolution of the polarization along the contour [51–53]. It is also known as the *Pancharatnam-Berry* (PB) phase, which is an important phase in optical and quantum fields [52–54].

We can think of the contour as a closed curve in the 2D polarization field, or as a closed curve on the Poincaré sphere. Let us recall how we had defined in section 2 the polar angle and the azimuthal angle

$$\cos\delta = s_3 = \frac{|E^+|^2 - |E^-|^2}{|E^+|^2 + |E^-|^2} \qquad \mu = \arctan\frac{s_2}{s_1} = \arg(E^{+*}E^-) = \alpha^- - \alpha^+. \tag{4.6}$$

Therefore, we can rewrite the geometric phase (4.5) as

$$\Phi_G = -\frac{1}{2}\oint \cos\delta d\mu = \frac{1}{2}\Sigma_{\text{equat}}. \tag{4.7}$$

This equality indicates that Φ_G is numerically equal to half of the spherical area Σ_{equat} swept by the shortest geodesic line connecting the point on the contour and the equator of the Poincaré sphere. When the angle μ increases (decreases) the area of the northern hemisphere is counted as negative (positive), while the area of the southern hemisphere is counted with the opposite signs the area of the southern hemisphere is the opposite.

If the contour of the integral on the sphere does not enclose the poles, the area swept by the geodesic is equal to the oriented area enclosed by the contour. Nevertheless, each time the contour encloses the s_3 axis, the area Σ_{equat} differs from the area enclosed by $\mp 2\pi$ (depending on the direction in which the contour rotates). Then, the geometric phase makes a jump of $\pm\pi$ when the contour crosses a pole.

Note that the topological number N_C (3.1) counts the C-points enclosed by the contour in the real space, which is equal to the number of times that the contour crosses the poles on the Poincaré sphere

$$\Phi_G = \frac{1}{2}\Sigma^{\pm} \mp \pi N_C, \tag{4.8}$$

where $\Sigma^{\mp}$ is the oriented area on the sphere enclosed by the contour. In this case, the $\pm$ hyper index denotes the area above and below the contours including the north and south poles, respectively.

The PB phase can be defined differently in a way which is more convenient in some practical cases as we just use the corresponding closed area

$$\bar{\Phi}_G^{\pm} = \Phi_G \pm \Phi_C = \frac{1}{2}\oint(\pm 1 - \cos\theta)d\phi = \frac{1}{2}\Sigma^{\pm}. \tag{4.9}$$

Now, the $\bar{\Phi}_G^+$ phase is continuous when the Poincaré-sphere contour crosses the north poles and makes a 2π jump when it crosses the south pole, and the opposite for $\bar{\Phi}_G^-$.

Considering definitions (4.5) and (4.9) and taking into account (4.3) it follows that

$$\bar{\Phi}_G^+ \bmod 2\pi = \bar{\Phi}_G^- \bmod 2\pi = \Phi \bmod 2\pi. \tag{4.10}$$

Chapter 5

Results

In this chapter we will look at some types of fields with singularities and classify them using our tool and the previous theory. We have coded in *Mathematica* complex initial fields for the vectorial equations and evolved them following the theory in [48]. We check for every moment of evolution that the condition on the two components is fulfilled, which is otherwise straightforward. We use the evolved fields to construct fields with phase singularities in one channel (E^+ or E^-) or both. In this way we can study how their phases change separately as well as in the polarization field. In turn, these fields can be made to evolve along z to see if there is any change in the singularities and which ones. This toolbox can also be used to calculate the values D_I (3.2), D_C (3.3) and D_L(3.5) to classify the singularities with charge ± 1; and the integrals ϕ_C (3.1), ϕ_D (4.1), ϕ (4.4), ϕ_G (4.5) and $\phi_G^{\pm}$ (4.9) varying the radius of the integral curve, or leaving it fixed and varying the field evolving it by z.

5.1 Static fields

First we will look at the simplest singularities with $N_C = \pm 1$. To do this we will use the scattering modes from chapter 1 to leave an real field without singularity in one component and a complex field with a singularity with $N = 1$ [1] in the other (see Fig. 5.1).

In the field with charge 1 we can see how the phase increases to 2π, jumping to the left of the singularity and leaving it with an undefined phase. In this way we can create four types of polarization fields depending on the sign of the charge and whether it is in N^+ or N^-.

$$\begin{aligned} N^+ = +1 \rightarrow N_C = -1, \qquad & N^+ = -1 \rightarrow N_C = 1, \\ N^- = +1 \rightarrow N_C = 1, \qquad & N^- = -1 \rightarrow N_C = -1. \end{aligned} \tag{5.1}$$

As we can observe in Figures 5.2 and 5.3 , using the classification of chapter 3, we obtain lemon singularities when $N_C = 1$ and star when $N_C = -1$. Moreover, they are of the elliptic type since the function S_0 has a minimum at (0,0), so S_{0x} and S_{0y} are null. Therefore, in the equation (3.3) we only have the first squared term which is clearly positive, so they are

[1] For negative topological charges it would be similar except that instead of increasing, the phase decreases.

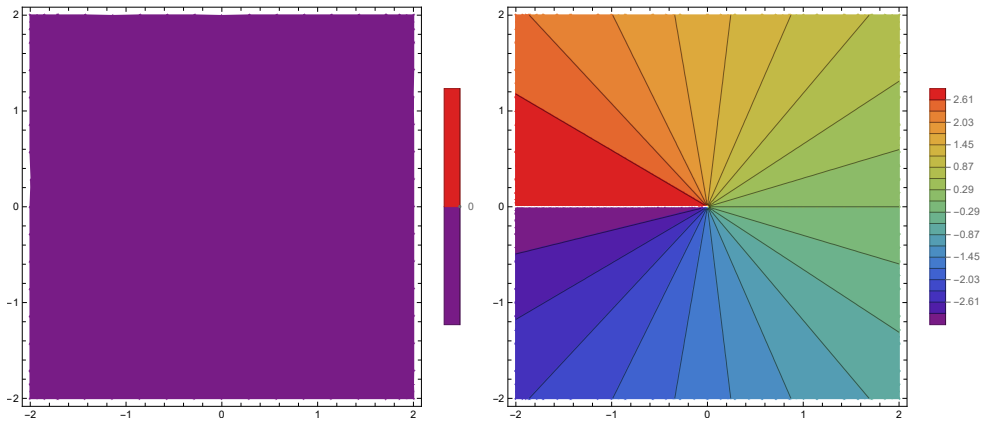

(a) (b)

Figure 5.1: Argument of scalar complex fields. (a) Field without any phase singularity. (b) Field with a phase singularity at the origin.

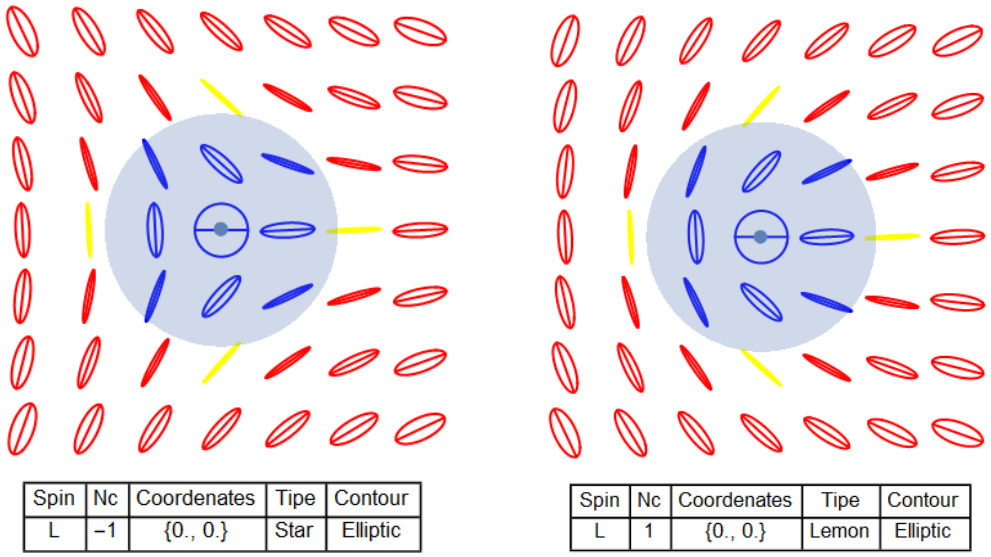

Spin	Nc	Coordenates	Tipe	Contour
L	−1	{0., 0.}	Star	Elliptic

Spin	Nc	Coordenates	Tipe	Contour
L	1	{0., 0.}	Lemon	Elliptic

Figure 5.2: Fields with LH singularities of charge +1 on (a) and -1 on (b), and below tables giving information on handedness, topological charge, coordinates of the singularity and the classifications according to lines and contour.

always elliptic singularities (because of the way we have constructed them).

We can also add singularities with a large topological charge in each of the channels to see how the polarization field changes. In these cases the pattern that emerges from the polarization field depends on the value of N_C, but not on the handedness of the singularities, for example in figure 5.5 it does not matter whether $N^+ = 4$ or $N^- = -4$ (in both cases

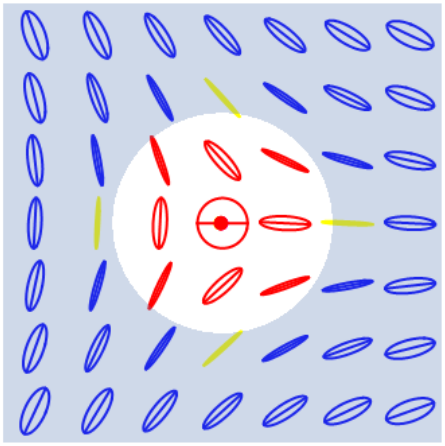

Spin	Nc	Coordenates	Tipe	Contour
R	1	{0., 0.}	Star	Elliptic

(a)

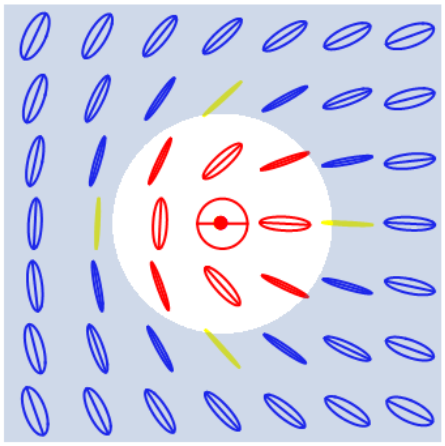

Spin	Nc	Coordenates	Tipe	Contour
R	1	{0., 0.}	Lemon	Elliptic

(b)

Figure 5.3: Fields with LH singularities of charge +1 on (a) and -1 on (b), and below tables giving information about handedness, topological charge, coordinates of the singularity and the classifications according to lines and contour.

$N_C = -4$). Therefore we will not differentiate between RH and LH. Thus, the different patterns that form the semi-major axes of the ellipses when $|N_C| = 2, 3$ and 4 are in figures 5.6, 5.7 and 5.8.

We have seen that the major axes of the ellipses around the circumference create different patterns depending on the value of N_C (3.1). So far, we have only created polarization singularities putting all the topological charge in one of the two channels (either in N^+ or in N^-) and leaving the other empty, but we can make combinations. The only restriction is that $|N^+| \neq |N^-|$, otherwise the value of S_3 (2.7) would cancel out and we would have linear singularities in the whole field.

Thus we can see that the aforementioned pattern only depends on the value of N_C, but the value of N_D can vary, which will have repercussions mainly on the eccentricity of the ellipses which will have an impact on the phases mentioned in chapter 4(see Fig.5.9, 5.10 and 5.11). The total charge on the circumferences becomes negative, we can see that the only continuous phase is ϕ_G^-, and the only one that varies depending on the value of N_D (4.1) is the total phase ϕ (4.4), which is why we define the other type of phases.

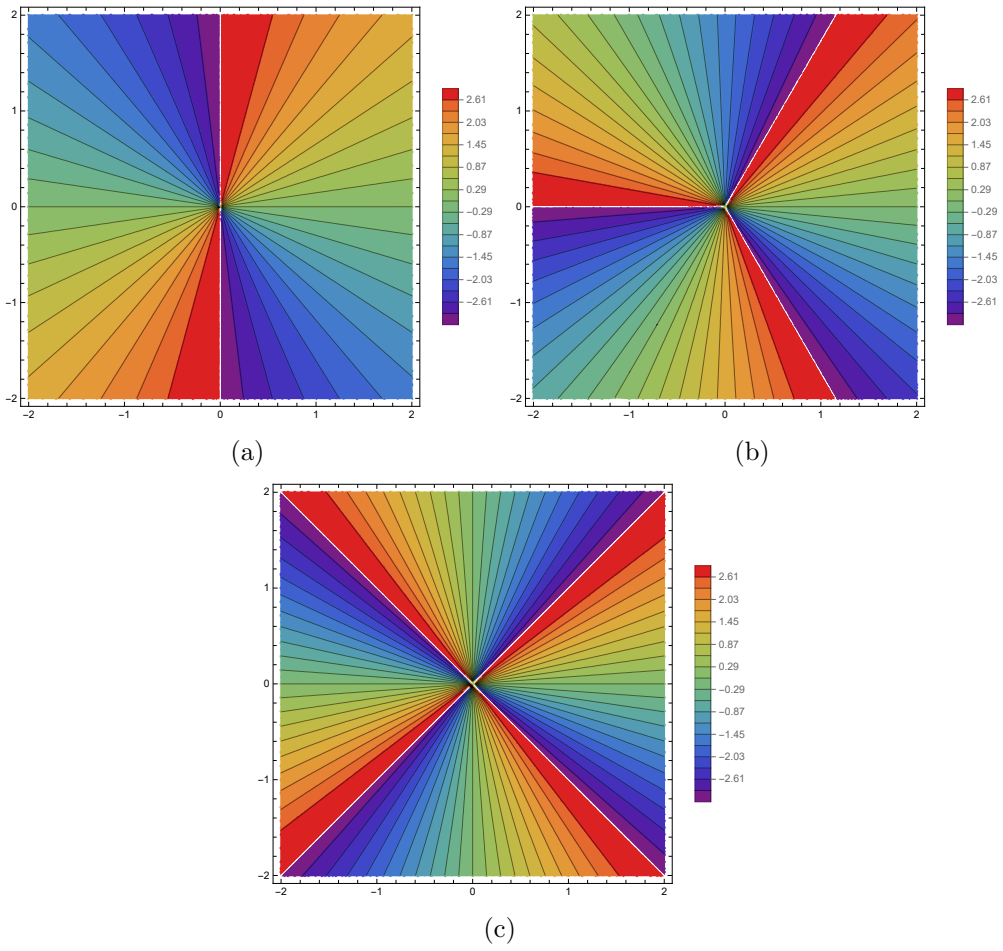

Figure 5.4: Argument of scalar complex fields. Fields with a phase singularities with charge 2 (a), with charge 3 (b) and with charge 4 (c).

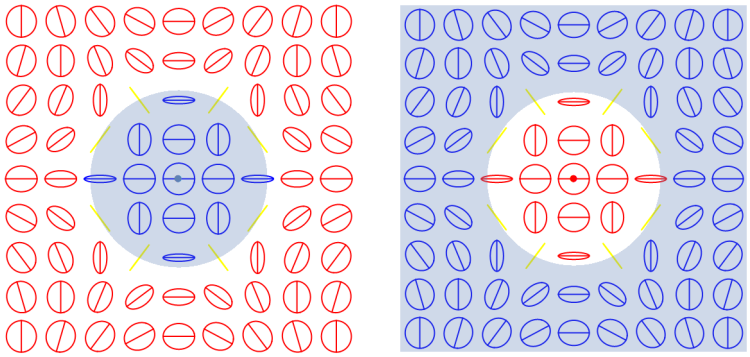

Figure 5.5: Singularity of different handedness with $N_C = -4$, but with the same pattern of semi-major axes.

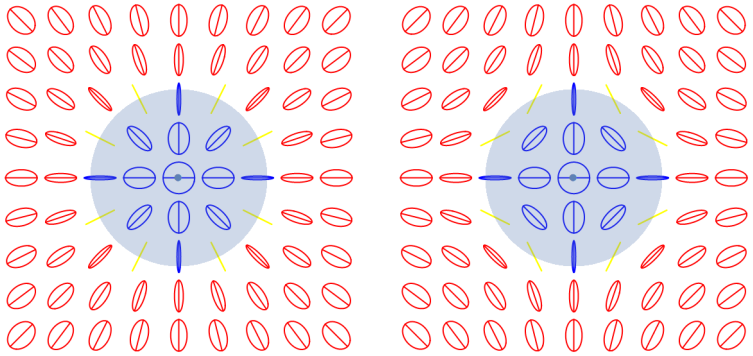

(a) (b)

Figure 5.6: Polarization fields with a LH C-point with $N_C = 2$ in (a) and $N_C = -2$ in (b).

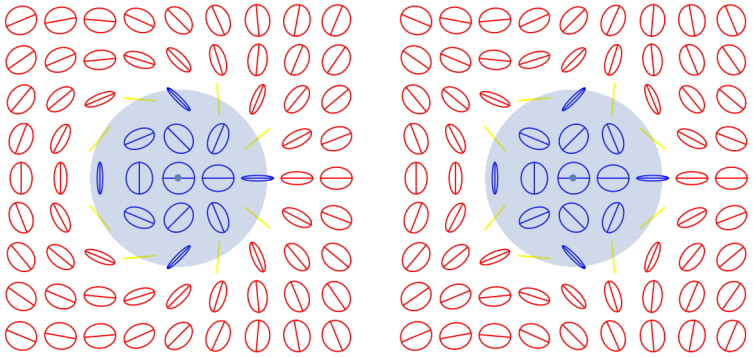

(a) (b)

Figure 5.7: Polarization fields with a LH C-point with $N_C = 3$ in (a) and $N_C = -3$ in (b).

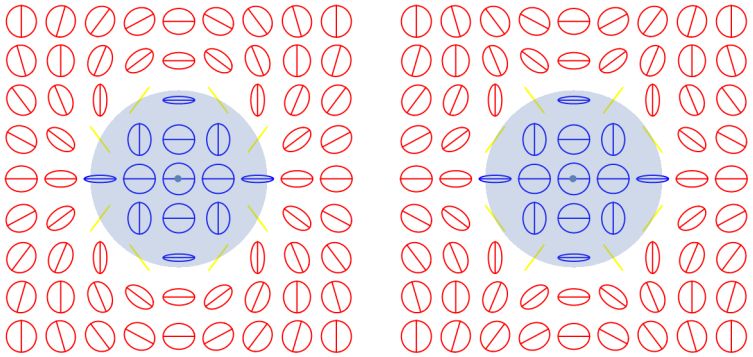

(a) (b)

Figure 5.8: Polarization fields with a LH C-point with $N_C = 4$ in (a) and $N_C = -4$ in (b).

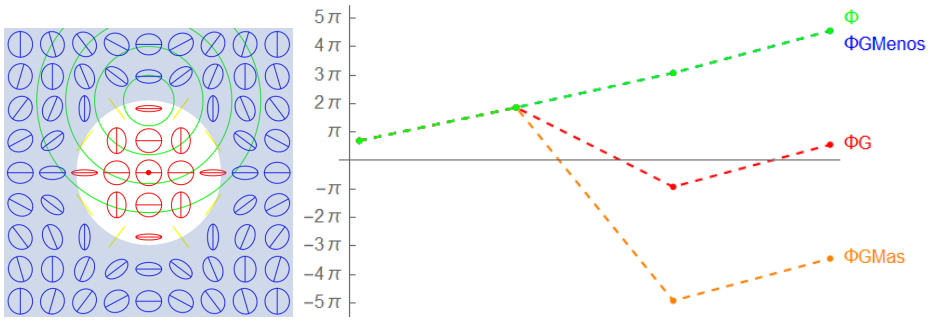

(a) (b)

Figure 5.9: (a) Complex field with a singularity with $N_C = -4$ and $N_D = -4 (N^- = -4$ and $N^+ = 0)$ and (b) value of the phases over circumferences centred at i and of radius R = 0.35, 0.75, 1.15 and 1.55.

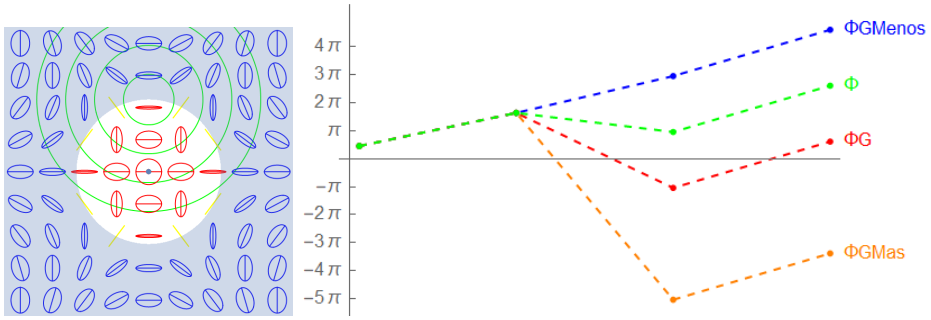

(a) (b)

Figure 5.10: (a) Complex field with a singularity with $N_C = -4$ and $N_D = -2 (N^- = -3$ and $N^+ = +1)$ and (b) value of the phases over circumferences centred at i and of radius R = 0.35, 0.75, 1.15 and 1.55.

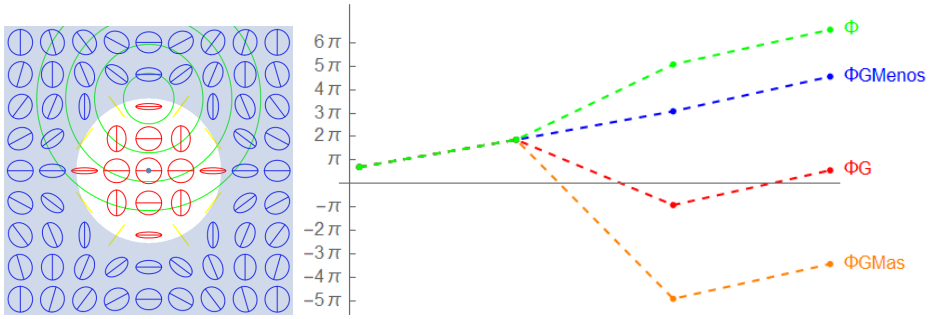

(a) (b)

Figure 5.11: (a) Complex field with a singularity with $N_C = -4$ and $N_D = -6 (N^- = -5$ and $N^+ = -1)$ and (b) value of the phases over circumferences centred at i and of radius R = 0.35, 0.75, 1.15 and 1.55.

5.2 Fields in evolution

The main reason for using the scattering modes seen in chapter 1 is that they allow us to be able to evolve the fields and how the singularities evolve or if and how they interact with each other.

In the case where we have an isolated singularity (regardless of its topological charge), it will not be able to interact with anything and its field will be significantly affected.

To see more dynamic fields, we first go to two separate singularities to see how they interact. We will put them in the three possible ways: (i) the two singularities in the same channel and with the same sign in the topological charge (see Fig. 5.12); (ii) the two singularities in the same channel and with opposite sign (see Fig. 5.13); and (iii) one singularity in each channel (see Fig. 5.14).

If we put two singularities with the same handedness and with the same sign in the topological charge, then the singularities will not interact with each other while evolving in z, as we can see in figure 5.12. On the other hand, looking at the figure 5.13, if the sign

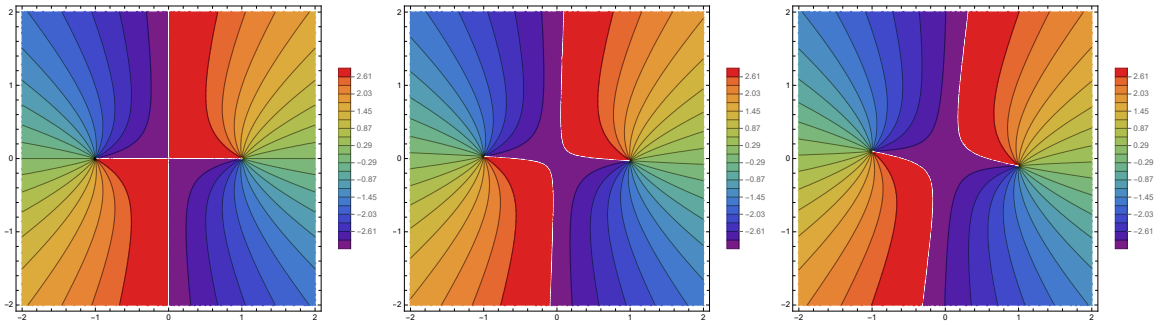

(a) (b) (c)

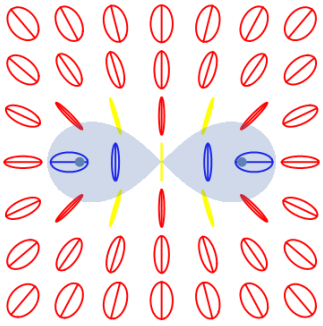

Spin	Nc	Coordenates	Tipe	Contour
L	1	{−1., 0.}	Lemon	Elliptic
L	1	{1., 0.}	Lemon	Elliptic

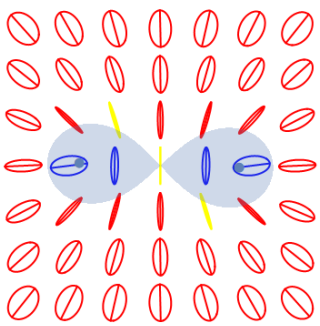

Spin	Nc	Coordenates	Tipe	Contour
L	1	{−1., 0.03}	Lemon	Elliptic
L	1	{1., −0.03}	Lemon	Elliptic

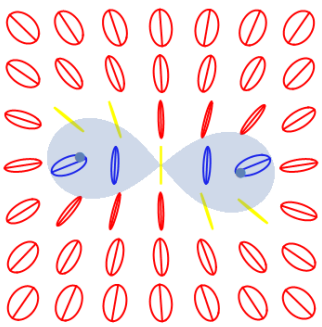

Spin	Nc	Coordenates	Tipe	Contour
L	1	{−1., 0.1}	Lemon	Elliptic
L	1	{1., −0.1}	Lemon	Elliptic

(d) (e) (f)

Figure 5.12: (a), (b) and (c) are the argument of the E^- component at $z = 0, 4$ and 6 respectively. (d), (e) and (f) are the polarization field with two singularities with topological charge with same sign at $z = 0, 4$ and 6 respectively.

of the topological charge is opposite, then the singularities will act as a particle-antiparticle pair attracting and destroying each other.

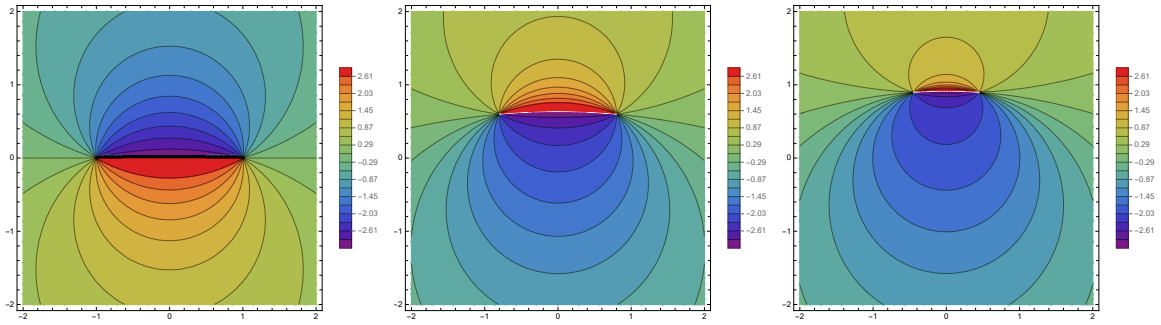

(a) (b) (c)

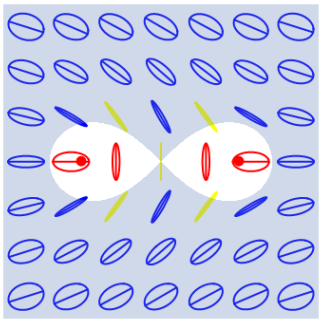

Spin	Nc	Coordenates	Tipe	Contour
R	1	{−1., 0.}	Lemon	Elliptic
R	−1	{1., 0.}	Star	Elliptic

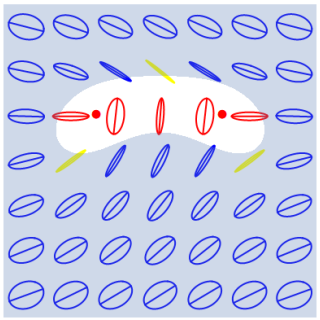

Spin	Nc	Coordenates	Tipe	Contour
R	1	{−0.80352, 0.59662}	Lemon	Elliptic
R	−1	{0.80352, 0.59662}	Star	Elliptic

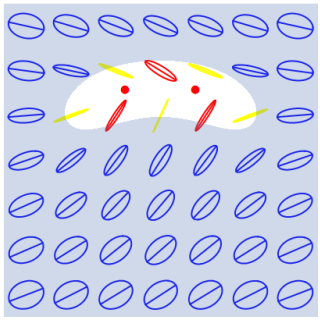

Spin	Nc	Coordenates	Tipe	Contour
R	1	{−0.450223, 0.89493}	Monstar	Elliptic
R	−1	{0.450223, 0.89493}	Star	Elliptic

(d) (e) (f)

Figure 5.13: (a), (b) and (c) are the argument of the E^+ component at $z = 0, 4$ and 6 respectively. (d), (e) and (f) are the polarization field with two singularities with topological charge with different sign at $z = 0, 4$ and 6 respectively.

However, when the singularities are each one with a handedness in figure 5.14, they will not interact with each other in any way, no matter what charges they have, but they will change the field around them.

In this way we can create an initial configuration with singularities of different types and with different charges in the field to see how they evolve and interact with each other (see Fig. 5.15). And, finally, if we are interested in a particular area, we are also able to make a fixed loop at that location in the field and evolve the field in z to see how the phases change in that loop (see Fig. 5.16).

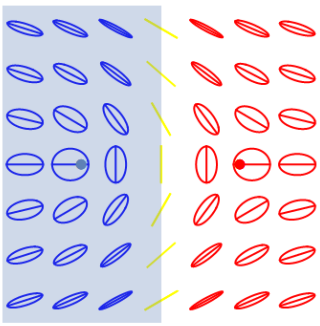

Spin	Nc	Coordenates	Tipe	Contour
R	−1	{1., 0.}	Star	Elliptic
L	1	{−1., 0.}	Lemon	Elliptic

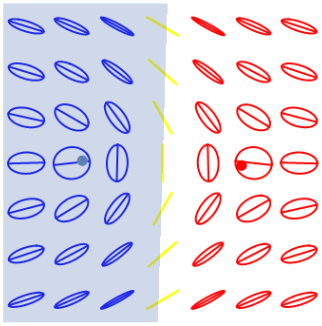

Spin	Nc	Coordenates	Tipe	Contour
R	−1	{1., −0.03}	Star	Elliptic
L	1	{−1., 0.03}	Lemon	Elliptic

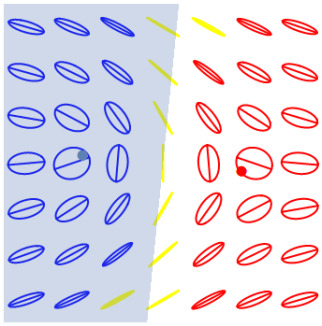

Spin	Nc	Coordenates	Tipe	Contour
R	−1	{1., −0.1}	Star	Elliptic
L	1	{−1., 0.1}	Lemon	Elliptic

Figure 5.14: Polarization field with two singularities with different handedness at $z = 0, 5, 10$.

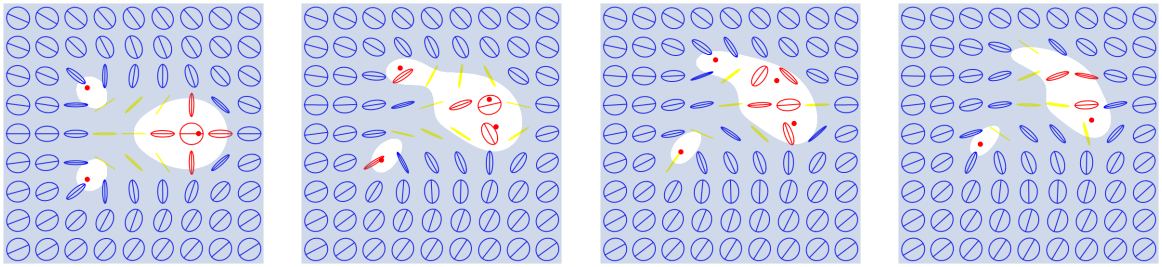

Figure 5.15: Evolution of a polarization field with two singularities of $N_C = +1$ at $\frac{-1+i}{\sqrt{2}}$ and $\frac{-1-i}{\sqrt{2}}$, and one with $N_C = -2$ at 1 for $z = 0, 1, 1.5, 2$.

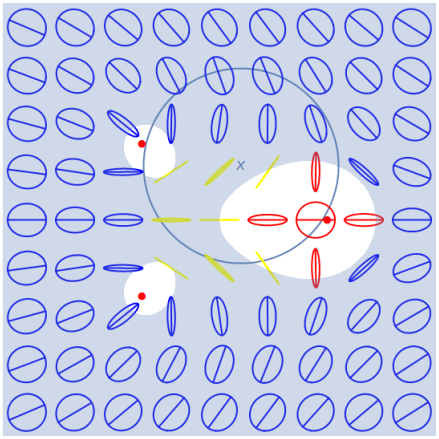

(a)

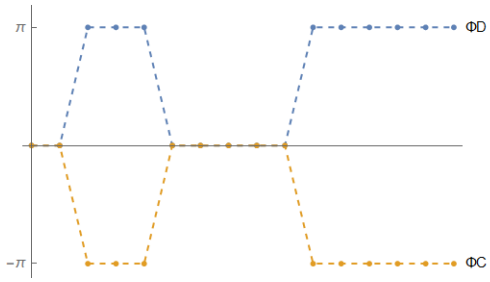

(b)

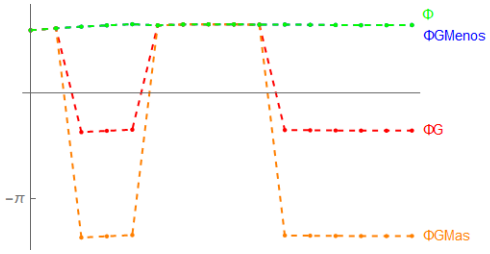

(c)

Figure 5.16: (a) Initial field configuration with a loop at (0.2,0.5) of radius 0.9. (b) Phases ϕ_C and ϕ_D changing along z between 0 and 2. (c) Phases ϕ, ϕ_G, ϕ_G^- and ϕ_G^- changing along z between 0 and 2.

Chapter 6

Conclusions

In this Master Thesis we studied the non-separable paraxial complex vector fields which model the propagation of an optical fields in an axially symmetric system, such as an optical fiber. For this we first detailed the mathematical formalism which describes the propagation of light in a fiber in the case of monochromatic beams, paraxial approximation and fixed polarization. The key differential equation describing this case is known as the Paraxial wave equation describing the propagation of the scalar optical field. We described briefly the dynamical evolution of multisingular initial beams within this formalism, a problem that can be solved analytically, introducing a set of polynomials which help solve the problem with a handleable recipe. This technique is reminiscent of other ways of solving parabolic or other Partial differential equations using appropriate sets of functions.

We then considered a generalization of this system, where polarization is not fixed. This means that instead of considering the scalar case we considered the vectorial case. We derived the partial differential equations describing this case, which now are a set of two equations for two of the components of the field plus a bound condition which permits to obtain the third component. The initial condition we considered showed one or many singularities in at least one of the components. We also discussed a second kind of singularities which only appear in the vectorial case, the polarization singularities. We discussed how to define their charge and how to represent and classify them.

With this theory at hand we developed a code in mathematica able to generate any multisingular condition in each component, perform its dynamical evolution and represent both the phase and polarization singularities. We then performed a systematic study of the relationship between the initial phase singularities and the associated polarization singularities and how they evolve dynamically. We found merging and disintegration of singularities with high charge and its relationship with the polarization singularities.

Thus we discussed the different patterns that emerge from the static fields and that how we can generate them in different ways, with the consequences that this has on the corresponding phase field. We also were able to simulate the dynamics of the fields along z to see how the singularities interact; destroying each other when they are in the same channel and have topological charge of opposite signs, and ignoring each other in the other cases. And finally to be able to study the different phases with respect to a fixed loop as the

field evolves.

In summary we have designed a tool that allows one to make analyze phase and polarization singularities in vectorial optical fields. Since these singularities appear in other fields, this tool is also useful for other systems, e.g. vortices two component Bose-Einstein condensates. As an outlook, we plan to use it to study systems with discrete symmetries, such as photonic crystal fibers [55], where the discrete symmetry introduces some constraints in the solutions and evolution of multisingular initial beams [56]. A second line of research will be to consider time or z dependent structures with discrete symmetries (i.e. a external potential in the case of Bose-Einstein condensate where evolution occurs in time, and a twisted photonic crystal fibers [57]. This directly will draw the results built with the tool presented in this Master Thesis to the edge of the current research in topological photonics [37]. Finally, this tool can easily be extended to the non-linear case, where the dynamics of singularities is very different than i the linear case, often hindering the merging of the singularities, and introducing a repulsion among singularities of the same sign, similarly as charge particles [58, 59].

Bibliography

[1] P. Bartha, *Analogy and analogical reasoning* (2013).

[2] D. Schlimm, *Two ways of analogy: Extending the study of analogies to mathematical domains*, Philosophy of Science 75 (2008) 178.

[3] O. Darrigol, *The analogy between light and sound in the history of optics from the Ancient Greeks to Isaac Newton. Part 1*, Centaurus 52 (2010) 117.

[4] O. Darrigol, *The Analogy between Light and Sound in the History of Optics from the ancient Greeks to Isaac Newton. Part 2*, Centaurus 52 (2010) 206.

[5] D. Dragoman, M. Dragoman, *Quantum-classical analogies*, 2013.

[6] Z. Cao, C. Yin, *Analogy Between Quantum Mechanics and Optics*, in: Advances in One-Dimensional Wave Mechanics, 2014, p. 1.

[7] M. Bunge, *Analogy in quantum theory: From insight to nonsense*, The British Journal for the Philosophy of Science 18 (1968) 265.

[8] R. J. Spreeuw, *Classical wave-optics analogy of quantum-information processing*, Physical Review A 63 (2001) 062302.

[9] S. Dehdashti, F. Yasar, *Oscillating between classically entangled state and separable state: an analogy between classical and quantum optics*, JOSA B 37 (2020) 2058.

[10] J. F. Nye, M. V. Berry, *Dislocations in wave trains*, in: A Half-Century of Physical Asymptotics and Other Diversions: Selected Works by Michael Berry, 1974, p. 6.

[11] V. Y. Bazhenov, M. Vasnetsov, M. Soskin, *Laser beams with screw dislocations in their wavefronts*, Jetp Lett 52 (1990) 429.

[12] M. Berry, *Making waves in physics*, Nature 403 (2000) 21.

[13] G. I. Taylor, *The mechanism of plastic deformation of crystals. Part I.—Theoretical*, Proceedings of the Royal Society of London. Series A, Containing Papers of a Mathematical and Physical Character 145 (1934) 362.

[14] M. Polanyi, *Form of lattice distortion that may render a crystal plastic*, Z Physik 89 (1934) 660.

[15] P. Li, Z. Zhang, *Standing wave effect and fractal structure in dislocation evolution*, Scientific reports 7 (2017) 1.

[16] Y. Guo, A. S. Tahvildar-Zadeh, *Formation of singularities in relativistic fluid dynamics and in spherically symmetric plasma dynamics*, Contemp. Math 238 (1999) 151.

[17] H. Moffatt, *Singularities in fluid mechanics*, Physical Review Fluids 4 (2019) 110502.

[18] L. Coy, E. R. Nash, P. A. Newman, *Meteorology of the polar vortex: Spring 1997*, Geophysical Research Letters 24 (1997) 2693.

[19] M. Soskin, M. Vasnetsov, *Singular optics*, Progress in optics 42 (2001) 219.

[20] M. Soskin, S. V. Boriskina, Y. Chong, M. R. Dennis, A. Desyatnikov, *Singular optics and topological photonics* (2016).

[21] M. Dennis, K. O'Holleran, M. Padgett, *Chapter 5 Singular Optics: Optical Vortices and Polarization Singularities, vol. 53* (2009).

[22] L. Allen, M. W. Beijersbergen, R. Spreeuw, J. Woerdman, *Orbital angular momentum of light and the transformation of Laguerre-Gaussian laser modes*, Physical review A 45 (1992) 8185.

[23] M. Soskin, V. Gorshkov, M. Vasnetsov, J. Malos, N. Heckenberg, *Topological charge and angular momentum of light beams carrying optical vortices*, Physical Review A 56 (1997) 4064.

[24] S. Franke-Arnold, L. Allen, M. Padgett, *Advances in optical angular momentum*, Laser & Photonics Reviews 2 (2008) 299.

[25] L. Paterson, M. P. MacDonald, J. Arlt, W. Sibbett, P. Bryant, K. Dholakia, *Controlled rotation of optically trapped microscopic particles*, Science 292 (2001) 912.

[26] M. Soskin, M. Vasnetsov, *Nonlinear singular optics*, Pure and Applied Optics: Journal of the European Optical Society Part A 7 (1998) 301.

[27] M.-Á. García-March, A. Ferrando, M. Zacarés, J. Vijande, L. D. Carr, *Angular pseudomomentum theory for the generalized nonlinear Schrödinger equation in discrete rotational symmetry media*, Physica D: Nonlinear Phenomena 238 (2009) 1432.

[28] A. Ferrando, *Discrete-symmetry vortices as angular Bloch modes*, Physical Review E 72 (2005) 036612.

[29] A. Ferrando, M. Zacarés, M.-A. Garcia-March, *Vorticity cutoff in nonlinear photonic crystals*, Physical review letters 95 (2005) 043901.

[30] J. Leach, M. R. Dennis, J. Courtial, M. J. Padgett, *Vortex knots in light*, New Journal of Physics 7 (2005) 55.

[31] M. V. Berry, M. R. Dennis, *Knotted and linked phase singularities in monochromatic waves*, Proceedings of the Royal Society of London. Series A: Mathematical, Physical and Engineering Sciences 457 (2001) 2251.

[32] M. Berry, M. Dennis, *Knotting and unknotting of phase singularities: Helmholtz waves, paraxial waves and waves in 2 + 1 spacetime*, Journal of Physics A: Mathematical and General 34 (2001) 8877.

[33] M. R. Dennis, R. P. King, B. Jack, K. O'holleran, M. J. Padgett, *Isolated optical vortex knots*, Nature Physics 6 (2010) 118.

[34] L. Lu, J. D. Joannopoulos, M. Soljačić, *Topological photonics*, Nature photonics 8 (2014) 821.

[35] T. Ozawa, H. M. Price, A. Amo, N. Goldman, M. Hafezi, L. Lu, M. C. Rechtsman, D. Schuster, J. Simon, O. Zilberberg, et al., *Topological photonics*, Reviews of Modern Physics 91 (2019) 015006.

[36] E. Lustig, M. Segev, *Topological photonics in synthetic dimensions*, Advances in Optics and Photonics 13 (2021) 426.

[37] Y. Shen, X. Wang, Z. Xie, C. Min, X. Fu, Q. Liu, M. Gong, X. Yuan, *Optical vortices 30 years on: OAM manipulation from topological charge to multiple singularities*, Light: Science & Applications 8 (2019) 1.

[38] I. S. Aranson, L. Kramer, *The world of the complex Ginzburg-Landau equation*, Reviews of modern physics 74 (2002) 99.

[39] M. Brambilla, F. Battipede, L. Lugiato, V. Penna, F. Prati, C. Tamm, C. Weiss, *Transverse laser patterns. I. Phase singularity crystals*, Physical Review A 43 (1991) 5090.

[40] M. Brambilla, L. Lugiato, V. Penna, F. Prati, C. Tamm, C. Weiss, *Transverse laser patterns. II. Variational principle for pattern selection, spatial multistability, and laser hydrodynamics*, Physical Review A 43 (1991) 5114.

[41] M. Berry, M. Dennis, R. Lee Jr, *Polarization singularities in the clear sky*, New Journal of Physics 6 (2004) 162.

[42] G. Horváth, B. Bernáth, B. Suhai, A. Barta, R. Wehner, *First observation of the fourth neutral polarization point in the atmosphere*, JOSA A 19 (2002) 2085.

[43] J. Gál, G. Horváth, V. B. Meyer-Rochow, R. Wehner, *Polarization patterns of the summer sky and its neutral points measured by full–sky imaging polarimetry in Finnish Lapland north of the Arctic Circle*, Proceedings of the Royal Society of London. Series A: Mathematical, Physical and Engineering Sciences 457 (2001) 1385.

[44] V. Ushenko, L. Trifonyuk, Y. Ushenko, O. Dubolazov, M. Gorsky, A. Ushenko, *Polarization singularity analysis of Mueller-matrix invariants of optical anisotropy of biological tissues samples in cancer diagnostics*, Journal of Optics 23 (2021) 064004.

[45] M. Dennis, *Polarization singularities in paraxial vector fields: morphology and statistics*, Optics Communications 213 (2002) 201.

[46] K. Y. Bliokh, M. A. Alonso, M. R. Dennis, *Geometric phases in 2D and 3D polarized fields: geometrical, dynamical, and topological aspects*, Reports on Progress in Physics 82 (2019) 122401.

[47] M. Berry, J. Hannay, *Umbilic points on Gaussian random surfaces*, Journal of Physics A: Mathematical and General 10 (1977) 1809.

[48] A. Ferrando, M. García-March, *Analytical solution for multi-singular vortex Gaussian beams: the mathematical theory of scattering modes*, Journal of Optics 18 (2016) 064006.

[49] J. F. Nye, *Lines of circular polarization in electromagnetic wave fields*, Proceedings of the Royal Society of London. A. Mathematical and Physical Sciences 389 (1983) 279.

[50] A. Thorndike, C. Cooley, J. F. Nye, *The structure and evolution of flow fields and other vector fields*, Journal of Physics A: Mathematical and General 11 (1978) 1455.

[51] A. Shapere, F. Wilczek, *Geometric phases in physics*, Vol. 5, 1989.

[52] S. Vinitskiĭ, V. L. Derbov, V. M. Dubovik, B. Markovski, Y. P. Stepanovskiĭ, *Topological phases in quantum mechanics and polarization optics*, Soviet Physics Uspekhi 33 (1990) 403.

[53] K. Y. Bliokh, *Geometrodynamics of polarized light: Berry phase and spin Hall effect in a gradient-index medium*, Journal of Optics A: Pure and Applied Optics 11 (2009) 094009.

[54] Y. Ben-Aryeh, *Berry and Pancharatnam topological phases of atomic and optical systems*, Journal of Optics B: Quantum and Semiclassical Optics 6 (2004) R1.

[55] P. Russell, *Photonic crystal fibres*, in: Optical Fiber Communication Conference, Optical Society of America, 2009, p. OTuC1.

[56] M.-Á. García-March, A. Ferrando, M. Zacarés, S. Sahu, D. E. Ceballos-Herrera, *Symmetry, winding number, and topological charge of vortex solitons in discrete-symmetry media*, Physical Review A 79 (2009) 053820.

[57] P. S. J. Russell, R. Beravat, G. Wong, *Helically twisted photonic crystal fibres*, Philosophical Transactions of the Royal Society A: Mathematical, Physical and Engineering Sciences 375 (2017) 20150440.

[58] A. L. Fetter, J. D. Walecka, *Quantum theory of many-particle systems*, 2012.

[59] K. A. Commeford, M. A. Garcia-March, A. Ferrando, L. D. Carr, *Symmetry breaking and singularity structure in Bose-Einstein condensates*, Physical Review A 86 (2012) 023627.